Engineering Structures 311 (2024) 118184

Contents lists available at ScienceDirect

Engineering Structures

journal homepage: www.elsevier.com/locate/engstruct

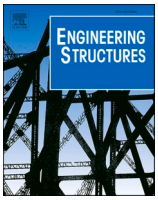

Deep learning-based prediction of structural responses of RC slabs subjected to blast loading

Xiao-Qing Zhou [a], Bing-Gui Huang [b,*], Xiao-You Wang [b], Yong Xia [b]

[a] College of Civil and Transportation Engineering, Shenzhen University, China
[b] Department of Civil and Environmental Engineering, The Hong Kong Polytechnic University, Hong Kong, China

ARTICLE INFO

Keywords:
Deep learning
Blast loading
RC slabs
Maximum displacement
Failure mode

ABSTRACT

Considering the risk of explosion, studying the dynamic structural behavior of reinforced concrete (RC) slabs subjected to blast loads is crucial for enhancing their resistance. Conventional approaches, including costly experimental tests, highly hypothetical analytical methods, and time-consuming numerical simulations, have their limitations. This study presents two deep learning-based models for rapid and accurate prediction of explosion-induced responses in RC slabs. Available literature data and supplemented numerical simulation data are used for training and testing. First, a multi-layer perceptron (MLP) model is established to predict the maximum displacement of RC slabs subjected to explosions. The input features include 10 parameters. The training results show that the MLP model exhibits good prediction performance. Second, a one-dimensional convolutional neural network (1D-CNN) model is constructed to predict the failure modes of RC slabs under explosive loads. The input features of the model are consistent with those of the MLP model. The 1D-CNN model outperforms the other five conventional machine learning models in classification. Furthermore, a permutation feature importance analysis is conducted to determine the effects of the 10 input features on the predicted outcomes. This analysis makes the predictions interpretable, thereby bolstering the credibility of the models. Results show that the proposed deep learning models offer an efficient and reliable method to predict the structural response of RC slabs under explosion loads.

1. Introduction

Explosive events, whether resulting from terrorist attacks or accidental occurrences, can lead to varying degrees of destruction and pose a threat to structural safety, resulting in potential casualties and severe loss of property [1]. Reinforced concrete (RC) slabs are one of the essential structural components of building structures [2]. When subjected to blast loads, RC slabs are prone to damage, resulting in stiffness degradation and intensified response, thereby exacerbating the severity of disasters. Therefore, developing a method is necessary to predict the structural behavior of RC slabs under explosions efficiently and accurately. In turn, it will help develop blast-resistant design strategies to reduce casualties and mitigate economic losses.

Experimental tests, analytical methods, and numerical simulations are typical methods used to analyze the explosion behavior of RC slabs. Conducting large-scale on-site explosion tests to study the structural responses of RC components is impractical due to high cost and complexity. Consequently, theoretical analysis and numerical simulations have become popular approaches.

Normally, theoretical analysis relies on the assumption of single-degree-of-freedom (SDOF) systems. SDOF systems are commonly employed to assess the flexural failure of components. For instance, Li & Meng [3] obtained normalized pressure impulse (P-I) curves based on the SDOF assumption using a maximum displacement-based damage criterion. However, real structures may exhibit other failure modes, thereby necessitating improved methods. Wang et al. [4] developed a simplified approach to derive the P-I curve of RC slabs under blast loads, considering different failure modes and degrees. Ma et al. [5] presented a method for determining the P-I curve of RC beams, considering bending and shear failure. Multi-degree-of-freedom (MDOF) systems have also been utilized. El-Dakhakhni et al. [6] used the MDOF framework to predict the failure modes of RC components subjected to explosive loads. Although this theoretical analysis method exhibits computational efficiency, its application is limited by excessive assumptions that complicate its usability in complex situations.

Numerical simulation, which mainly adopts the finite element (FE)

* Corresponding author.
E-mail address: binggui.huang@connect.polyu.hk (B.-G. Huang).

https://doi.org/10.1016/j.engstruct.2024.118184
Received 2 November 2023; Received in revised form 18 March 2024; Accepted 9 May 2024
Available online 21 May 2024

method, is another widely used approach for analyzing the structural behavior of RC slabs under explosive loads. Some studies focused on investigating the structural behavior of RC slabs. For example, Syed et al. [7] examined the damage and failure modes of RC slabs under near-field and far-field explosions. Zhou et al. [8] employed a concrete dynamic plasticity failure material model to explore the dynamic response of RC slabs. Moreover, some studies examine the effects of various factors on the structural response. Senthil et al. [9] analyzed the effects of TNT weight, standoff distance, and boundary conditions on the damage mechanisms. Jia et al. [10] investigated the effect of explosive weight and position on the damage modes of two-way RC slabs.

Despite the effectiveness of the numerical simulation, it requires expertise in configuring material models, mesh sizes, boundary conditions, and other parameters. Furthermore, analyzing the dynamic response of refined models is extremely time-consuming. Therefore, efficient methods have been developed. For example, based on numerical results, Zhao et al. [11] developed formulas to assess the maximum displacement of RC slabs under blast loads. Li et al. [12] adopted formulas to determine the P-I curve of RC slabs. However, the empirical equations are only applicable to specific RC slabs. The dynamic response of RC slabs subjected to explosive loads is influenced by various factors, thereby presenting challenges in establishing accurate and universal empirical formulas. Therefore, the utilization of machine learning (ML) with robust data processing capabilities is proposed to address this issue.

ML techniques have been proven efficient and effective in addressing challenges in civil engineering. For instance, Lai et al. [13] and Jueyendah et al. [14] developed predictive models to estimate the maximum displacement of RC beams under impact loads and predict the mechanical properties of cement mortar, respectively. Naderpour et al. [15] developed a model to predict the seismic failure modes of RC columns. Li et al. [16] attempted to predict the structural behavior under dynamic loads using graph neural networks. Several studies have also been conducted to assess the blast-induced damage of slabs. Almustafa & Nehdi [17,18] satisfactorily evaluated the maximum displacement of RC slabs and fiber-reinforced polymer-reinforced slabs under blast loads using the random forest (RF) and Gaussian process regression (GPR) algorithms. Zhao et al. [19] developed support vector machine (SVM), GPR, RF, and back propagation neural network algorithms to assess the maximum displacement of RC slabs. However, focusing solely on the maximum displacement of slabs under explosive loads is insufficient. Examining the failure modes of slabs subjected to explosions is equally important for a better understanding of the structural behavior.

Deep learning (DL), a vital branch of ML, has gained widespread popularity because of its strong feature extraction capabilities and excellent prediction performance. The application of DL techniques has demonstrated exceptional performance across various fields, including damage detection [20], time-domain data processing [21], construction classification [22], concrete strength prediction [23], image analysis of concrete pore structure [24], and identification of earthquakes and explosions [25]. However, very limited DL studies have been conducted on the dynamic response of RC structures under explosive loads. One critical challenge is the insufficient quantity of real test data for training. To the best knowledge of the authors, only our previous study [26] established two DL models to predict the responses of RC columns subjected to blast loads. No study on the responses of RC slabs is based on DL techniques under blast loads.

In this study, two DL models are developed to enable the rapid and precise prediction of the response of RC slabs under blast loads. The first model is the multi-layer perceptron (MLP) neural network. It is used to predict the maximum displacement of RC slabs under explosions. The input features include eight structural parameters and two explosion load parameters. The second model is the one-dimensional convolutional neural network (1D-CNN). It is used to predict the failure modes of RC slabs subjected to explosions. The proposed models are compared with five traditional ML models.

2. Database of RC slabs

2.1. Literature data

ML requires a considerable number of reliable data for training. However, the available test data are limited due to the high cost and spatial constraints of experiments. In this study, 77 data samples, including 16 data samples from field blast tests [27,30] and 61 data samples from numerical simulations [7,10,11,27,31,32] are collected. The data sources are presented in Table 1. The experimental data only consisted of one-way slabs with maximum displacements between 1.5 mm and 50 mm. Yao et al. [27] and Wang et al. [28,29] focused on the response of RC slabs subjected to close-in explosive loadings, whereas Wu et al. [30] studied the response under far-field blast loadings. The collected numerical simulation data included 30 samples of one-way slabs and 31 samples of two-way slabs, with maximum displacements ranging from 0.7 mm to 239 mm. Yao et al. [27] and Zhao et al. [11] analyzed the structural responses of RC slabs subjected to close-range explosions, contributing 16 data samples. Du & Li [31], Syed et al. [7], Jia et al. [10], and Abdel-Mooty et al. [32] focused on the structural behavior of slabs subjected to far-field explosions, resulting in 45 data samples. The detailed parameter ranges of the collected data are presented in Table 2.

2.2. Numerical simulation data

Due to the limited availability of literature data, the training dataset needs to be expanded. In this study, the structural behavior of RC slabs under various explosive conditions is simulated using the LS-DYNA software. The numerical models are validated, thereby expanding the training dataset.

2.2.1. Calibration of the FE model

Two different case studies are conducted to demonstrate the reliability of the numerical simulation. Case I uses experimental data from Wang et al. [28] to validate the accuracy of the constructed FE model in simulating the damage degree and maximum displacement of RC slabs under explosive loads. A comparison of displacement–time history between the experiment and the numerical simulation is unavailable because of the absence of displacement curve measurement in Case I. Therefore, in Case II, the experimental study by Su et al. [33] is used to validate the effectiveness of numerical simulation.

(1) Case I.

The dimensions of the RC slab [28] were 1100 mm × 1000 mm × 40 mm. The steel bars were arranged in a single layer along both directions with a spacing of 75 mm, a diameter of 6 mm, and a yield strength of 600 MPa. The compressive and tensile strengths of the concrete were 39.5 MPa and 4.2 MPa, respectively. The blast charge was placed in the center of the slab at a height of 0.4 m. The experimental setup is depicted in Fig. 1 [28].

Table 1
Sources of literature data.

Author	Year	Type	Number
Yao et al. [27]	2016	Experimental study	6
Wang et al. [28]	2013	Experimental study	4
Wang et al. [29]	2012	Experimental study	2
Wu et al. [30]	2009	Experimental study	4
Du & Li [31]	2009	Numerical simulation	9
Syed et al. [7]	2018	Numerical simulation	14
Yao et al. [27]	2016	Numerical simulation	7
Jia et al. [10]	2014	Numerical simulation	6
Abdel-Mooty et al.[32]	2014	Numerical simulation	16
Zhao et al. [11]	2019	Numerical simulation	9

Table 2
Range of literature data.

Feature	Unit	Symbol	Range	
			Experiment	Simulation
Length	m	L	0.85 ~ 2	0.85 ~ 3
Width	m	W	0.75 ~ 1.25	0.75 ~ 3
Thickness	m	T	0.03 ~ 0.1	0.03 ~ 0.16
Concrete compressive strength	MPa	f_c	39.5 ~ 40	13.7 ~ 140
Rebar yield strength	MPa	f_y	395 ~ 600	300 ~ 630
Rebar diameter	mm	D	6 ~ 12	5 ~ 12
Rebar spacing	mm	R	50 ~ 750	30 ~ 250
Charge mass	kg	M	0.13 ~ 8.2	0.13 ~ 1000
Blast distance	m	d	0.3 ~ 3	0.3 ~ 15
Type of slab	/	F	One-way	One-way, Two-way

Fig. 1. Experimental setup [28].

As shown in Fig. 2, a three-dimensional 1/4 of the slab is modelled to optimize computational efficiency for the numerical simulation. The rebar and concrete are modelled separately using a grid size of 3 mm, resulting in 399,464 concrete elements and 5248 reinforcement elements. A mesh size sensitivity analysis has been studied. The element size used here is selected by trading off the accuracy and efficiency. The K&C model [34] is adopted to model the concrete, incorporating the dynamic increase factor (DIF) of compressive strength proposed by CEB [35], whereas the DIF of tensile strength was adopted from the formulation presented by Malvar & Crawford [36]. The PLASTIC_KINEMATIC model [37] is adopted for the reinforcement, in which the DIF follows the formulation presented by Malvar & Crawford [38]. The boundary conditions of the slab are simulated by establishing rigid bodies and employing the automatic surface-to-surface contact method. The LOAD_BLAST method is used to apply the explosion. Tables 3 and 4 show the primary material parameters of the concrete and rebar, respectively.

The conditions on the rear surface of the slab after the detonation are shown in Fig. 3. Along with the emergence of radial cracks, localized concrete spalling is observed in the central region. The experiment results indicate that the radius of concrete spalling on the rear surface is approximately 120 mm, accompanied by a maximum displacement of 35 mm. Numerical simulations show similar damage conditions, revealing a rear surface spalling radius of 110 mm and a maximum displacement of 33.6 mm. These results exhibit deviations of 8% and 4.5% from the experimental values, respectively, which are well within an acceptable range. Additionally, numerical simulations are conducted for explosion cases of (0.2 kg, 0.4 m) and (0.31 kg, 0.4 m), and the results are presented in Table 5. The numerical results agree well with the experimental results. The aforementioned comparison demonstrates that the constructed numerical model can accurately simulate the damage extent and maximum displacement of RC slabs exposed to explosions.

(2) Case II.

To further validate the accuracy of the numerical simulation, an RC one-way slab labeled NSC-2 by Su et al. [33] is investigated. The dimensions of the slab were 2400 mm × 1000 mm × 100 mm. The steel bars were double-layered and arranged bidirectionally, with a diameter of 10 mm and a yield strength of 480 MPa. The spacing between the bars was 200 mm along the length side and 100 mm along the width side.

Table 3
Material parameters of concrete.

Density (kg/m^3)	Poisson ratio	Compressive strength (MPa)	b1	b2	b3
2500	0.2	39.5	0.8	6.35	0.3

Note: b1, b2, and b3 are damage parameters.

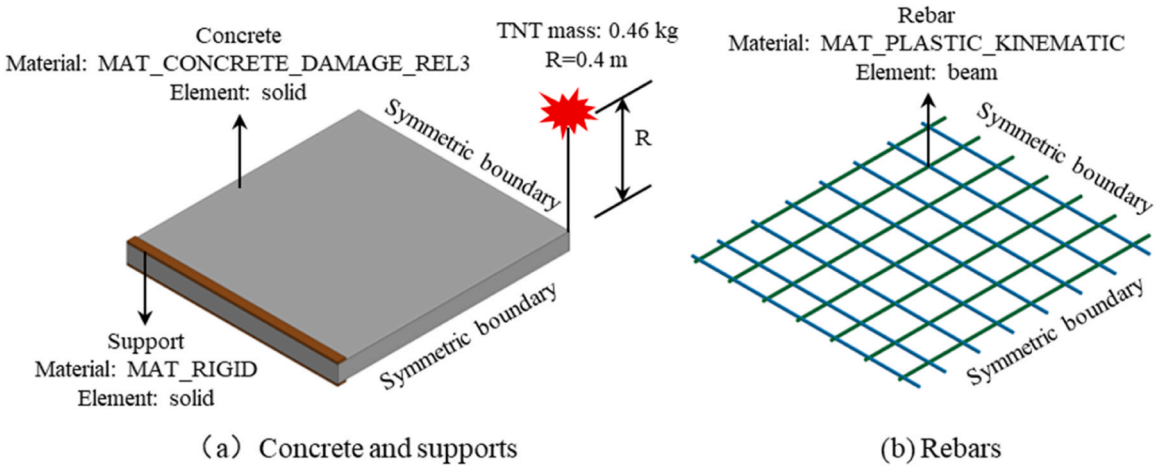

Fig. 2. FE model of Case I.

Table 4
Material parameters of rebar.

Density (kg/m^3)	Poisson ratio	Young's modulus (GPa)	Yield strength (MPa)	C	P
7830	0.3	200	600	40	5

Note: C and P are strain rate parameters.

The concrete compressive strength was 30.4 MPa. The blast charge, with a mass of 4 kg, was positioned at a height of 1.27 m from the center of the slab. The fixed constraints were located on both sides of the length edge of the slab. More detailed information can be found in Reference [33].

The FE model is established and illustrated in Fig. 4. Due to structural symmetry, a three-dimensional 1/4 model is adopted to reduce the computational time. The mesh size for concrete and steel bars is set to 10 mm, resulting in 60,000 concrete elements and 2140 steel elements. The material models employed in this case are identical to those in Case I. At the edge of the slab, cylindrical rigid bodies are created, and the CONTACT_NODES_TO_SURFACE algorithm is utilized to simulate the contact interface between the RC slab and the supports. Static and dynamic friction are defined as 0.3 and 0.2, respectively. Concrete damage parameters b1, b2, and b3 are used from Reference [33].

The experimental and FE simulation results of the deflection curve at the center of the slab are compared in Fig. 5. The numerical simulation results agree well with the experimental results. The maximum displacement measured in the experiment was 43.28 mm, and the residual deflection was 15.51 mm. The numerical simulation provides a maximum displacement of 39.4 mm and a residual deflection of 16.47 mm, resulting in a difference of 9% and 6%, respectively. Overall, the experimental and numerical simulation results show a considerable degree of consistency, indicating that the developed FE model can simulate the structural behavior of the slab exposed to blast effectively.

The reliability of the numerical model is verified based on the

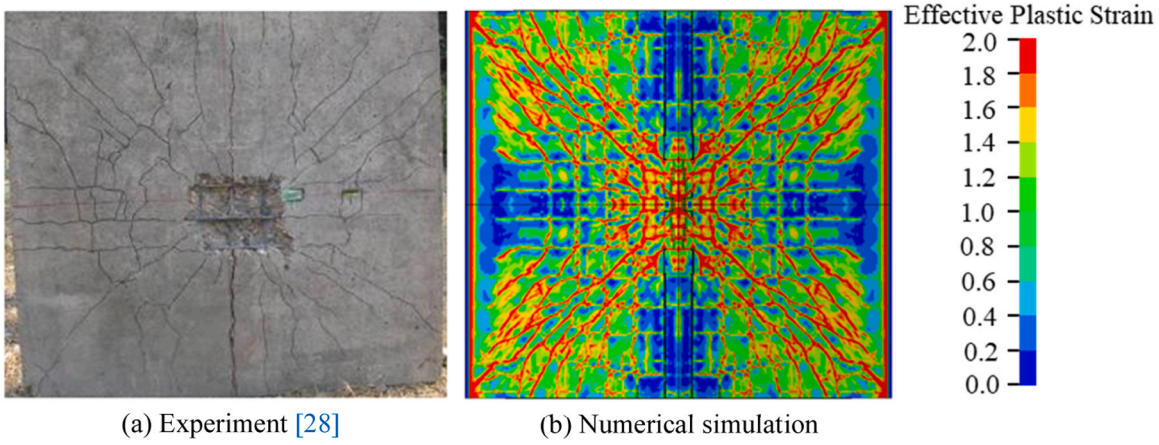

Fig. 3. Rear surface damage after explosion: numerical simulation vs. experiment.

Table 5
Slab maximum displacement: numerical simulation vs. experiment.

Dimension of the slab (mm)	Charge mass (kg)	Blast distance (m)	Scale distance (m/kg$^{1/3}$)	Maximum displacement (mm)		Deviation
				Experiment	Numerical simulation	
1100 × 1000 × 40	0.2	0.4	0.68	10.1	9.1	9.9%
	0.31	0.4	0.59	14.8	15.9	7.4%

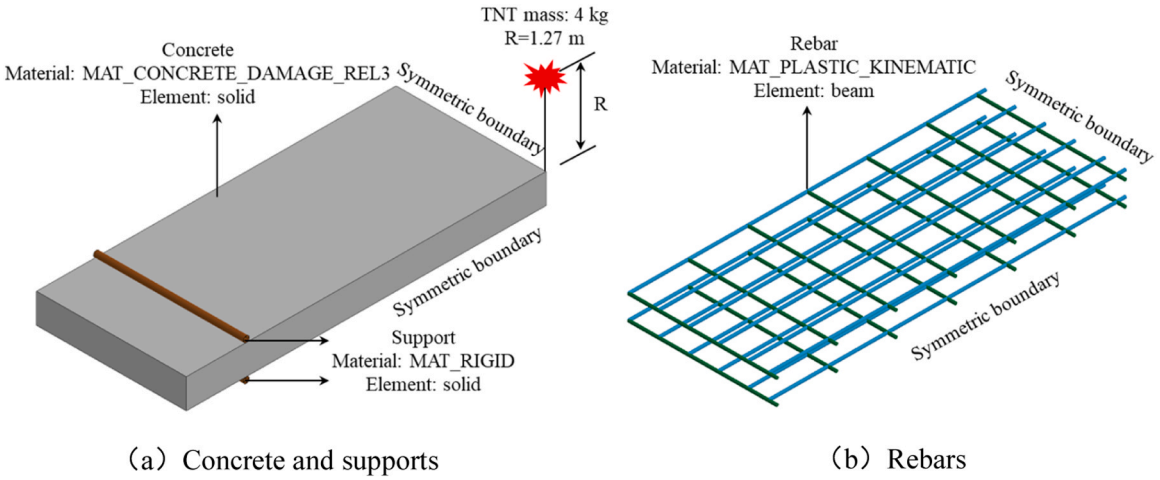

Fig. 4. FE model of Case II.

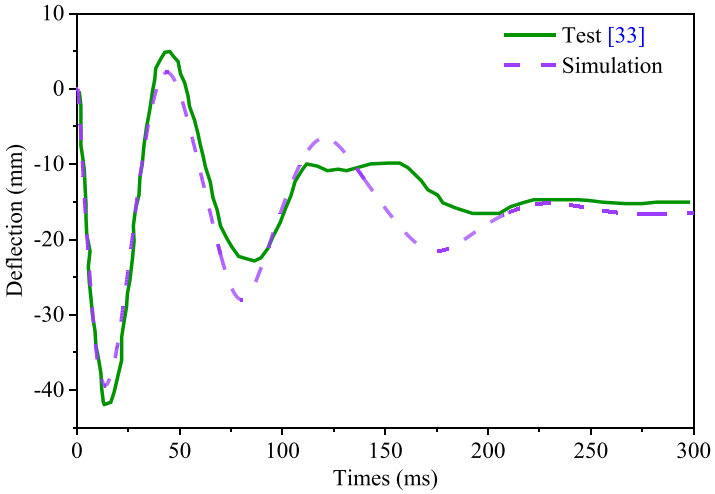

Fig. 5. Displacement–time history of the slab center.

aforementioned analysis. The dynamic response of different types of RC slabs under varying explosive loading cases will be simulated using the validated numerical model, thereby expanding the training dataset.

2.2.2. Supplementation of numerical simulation data

This section mainly concentrates on exploring the structural responses of RC slabs subjected to detonations caused by suitcase bombs and small vehicle bombs. The parameters of the explosion load are determined based on Reference [39], whereas the structural parameters of the RC slabs are determined in accordance with the Chinese design code [40]. A total of 495 data samples, including 270 single-way slabs and 225 two-way slabs, are supplemented. The dataset for one-way slabs contains a range of maximum displacements ranging from 3.8 mm to 1146 mm, whereas the dataset for two-way slabs contains maximum displacements ranging from 21.1 mm to 1101 mm. Detailed parameter ranges for the supplementary numerical simulation data are listed in Table 6. Notably, in the numerical models, the explosives are placed above the center of the slab, a single-layer reinforcement is configured with equal spacing in both directions, and fixed constraints are adopted.

During the manual processing of numerical simulation data, the failure modes of the RC slab are recorded systematically. Fig. 6 illustrates a damage example of an RC one-way slab under varying explosive loading conditions. The dimensions of the slab are 850 mm × 750 mm × 30 mm. Under the explosive loading of (5 kg, 3 m), (30 kg, 3 m), and (60 kg, 3 m), the slab exhibits bending failure (BF), bending-shear failure (BSF), and shear failure (SF), respectively. Different failure modes exhibit varying damage characteristics. For instance, SF is characterized by direct shear failure at the support locations.

Table 6
Parameter ranges for supplementary numerical simulation data.

Parameter	Variable	Symbol	Unit	Range
Length	x_1	L	m	3 ~ 5
Width	x_2	W	m	2 ~ 4
Thickness	x_3	T	m	0.05 ~ 0.2
Concrete compressive strength	x_4	f_c	MPa	30 ~ 60
Rebar yield strength	x_5	f_y	MPa	335 ~ 600
Rebar diameter	x_6	D	mm	6 ~ 12
Rebar spacing	x_7	R	mm	80 ~ 200
Charge mass	x_8	M	kg	5 ~ 300
Blast distance	x_9	d	m	1 ~ 3
Type of slab	x_{10}	F	/	one-way, two-way

2.3. Description of the dataset

This study contains 572 data samples, including 77 data samples collected from the literature and 495 supplementary numerical simulation data samples. Among them, 316 data samples are for one-way slabs, and 256 data samples are for two-way slabs. Table 7 presents the minimum, maximum, mean, and standard deviation values of these datasets.

3. Maximum displacement prediction DL model

In this section, an MLP model is developed to predict the maximum displacement of RC slabs exposed to explosive loads. The dataset consists of 418 samples, including 236 single-way slabs and 182 two-way slabs. Some samples that experience collapse failure are excluded from the training dataset because of the unavailability of maximum displacement measurements.

3.1. Configuration of MLP model

The performance of an MLP model relies on the configuration of its hyperparameters, such as the number of hidden layers and the corresponding number of neurons, learning rate, batch size, epochs, and activation function. Bayesian optimization exhibits superior efficiency in exploring hyperparameter space by utilizing prior information to guide the search direction [41]. Therefore, Bayesian optimization is used to determine the configuration of the MLP model.

In addition to hyperparameter optimization, the k-fold cross-validation [42] is used to estimate the performance of the model and select appropriate hyperparameters. The dataset is divided into k subsets, and k iterations are performed. In each iteration, k-1 subsets are used for model training, and the remaining subset is utilized for validation. Through iterative training and validation on different subsets, the k-fold cross-validation provides a comprehensive evaluation of the model's generalization capabilities. In this section, a 10-fold cross-validation method is employed, ensuring that the determined hyperparameters exhibit remarkable predictive capability.

The architecture of the MLP model comprises three hidden layers, each containing 20 neurons. The selected hyperparameters include a learning rate of 0.001, a batch size of 12, 1500 training epochs, and the utilization of the sigmoid activation function. The MLP model structure is shown in Fig. 7, where w represents the weight of the connection between two neurons, and b denotes the bias value. Variables x_1 to x_{10} correspond to the 10 input features listed in Table 6, while the output variable y represents the maximum displacement.

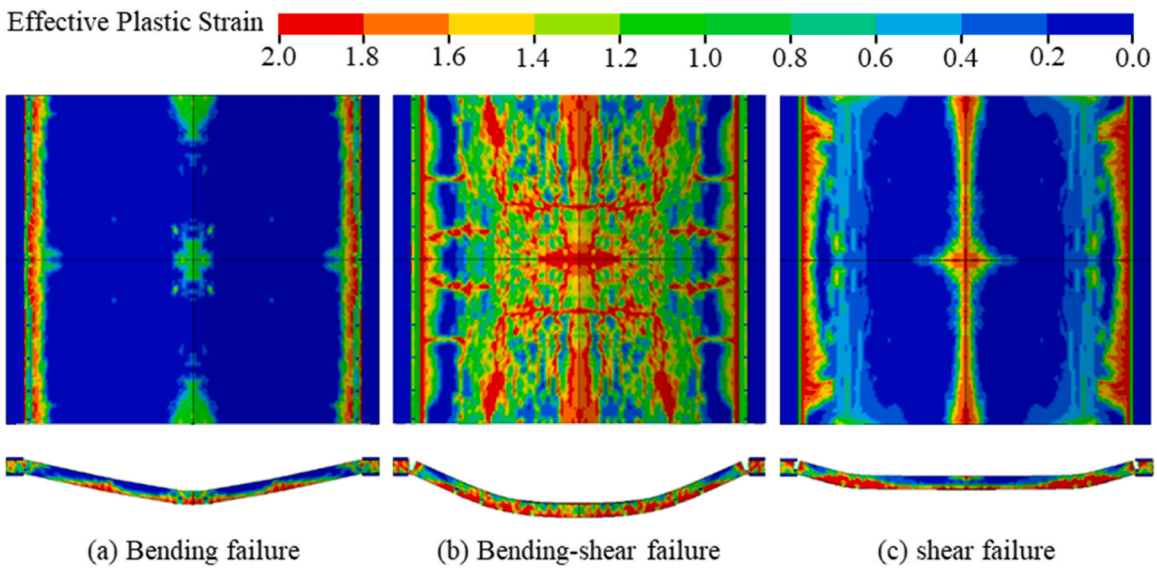

Fig. 6. Failure mode of RC slab (top view above, side view below).

Table 7
Minimum, maximum, mean, and standard deviation of the datasets.

Parameter	Minimum	Maximum	Mean	Standard deviation
Length	0.85	5	3.59	1.03
Width	0.75	4	2.72	0.81
Thickness	0.03	0.2	0.10	0.04
Concrete compressive strength	13.7	140	45.15	16.24
Rebar yield strength	300	630	418.79	79.24
Rebar diameter	5	12	9.38	2.48
Rebar spacing	30	750	111.21	45.13
Charge mass	0.13	1000	101.99	154.86
Blast distance	0.3	41	2.33	2.82
Maximum displacement	0.64	1146	243.68	251.34

3.2. Model training and results discussion

The datasets are trained using the MLP neural network configuration. The datasets are randomly split into three subsets, namely, a training set, a validation set, and a test set, comprising 293, 83, and 42 samples, respectively. Z-score normalization is applied to standardize the data, ensuring consistent feature scales to optimize model training efficiency and enhance convergence [43].

Fig. 8 shows the variation trend of the mean squared error (MSE) during the training process. The gradual decrease in MSE indicates that the model progressively learns the features of the data and moves toward more accurate prediction outcomes. Upon the completion of training, the MSE of the training set is 0.00725.

To assess the prediction performance of the model comprehensively, five widely utilized assessment metrics are employed on the training, validation, and test sets. These five metrics include the coefficient of determination (R^2), explained variance score (*EVS*), root mean squared error (*RMSE*), mean absolute error (*MAE*), and scatter index (*SI*), defined by Eqs. (1) to (5), respectively. Among these metrics, higher values of R^2 and *EVS* signify greater prediction accuracy, whereas lower values of *RMSE*, *MAE*, and *SI* indicate superior prediction performance.

$$R^2 = 1 - \frac{\sum_{i=1}^{n}(P_i - T_i)^2}{\sum_{i=1}^{n}(P_i - \overline{T})^2}, \tag{1}$$

$$EVS = 1 - \frac{Var\{T_i - P_i\}}{Var\{T_i\}}, \tag{2}$$

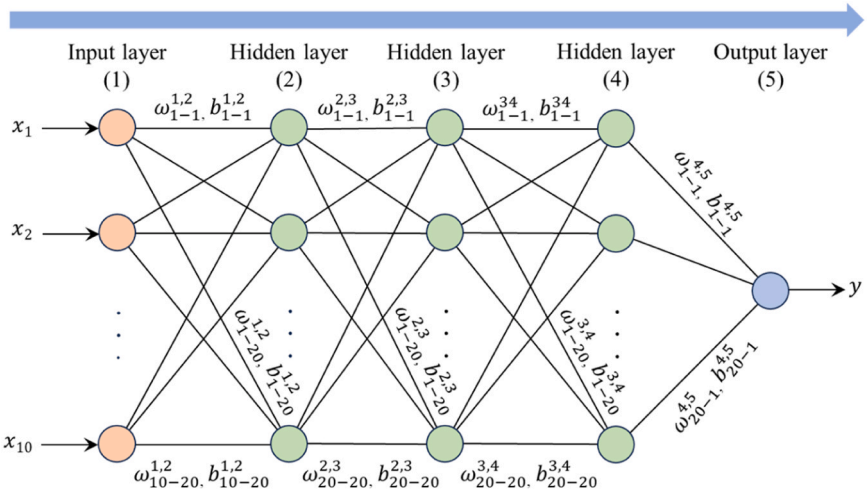

Fig. 7. Neural network structure of the MLP model.

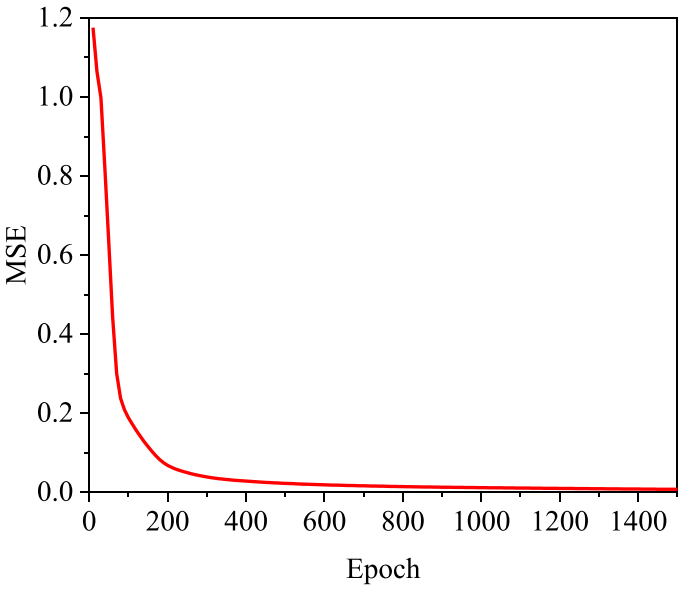

Fig. 8. Variation trend of MSE.

$$RMSE = \sqrt{\frac{\sum_{i=1}^{n}(P_i - T_i)^2}{n}}, \tag{3}$$

$$MAE = \frac{\sum_{i=1}^{n}|P_i - T_i|}{n}, \tag{4}$$

$$SI = \frac{\sqrt{\frac{1}{n}\sum_{i=1}^{n}(T_i - P_i)^2}}{\overline{T}}, \tag{5}$$

where P_i and T_i signify the predicted and actual values, respectively; $\overline{T}$ denotes the mean value of the actual values; *Var* represents the variance; and n is the number of samples.

Table 8 presents the performance of various evaluation metrics across different datasets. These metrics exhibit similar performance across the training, validation, and test sets. For instance, the R^2 values for the training, validation, and test sets are 0.9929, 0.9886, and 0.9923, respectively, indicating robust model generalization. Notably, R^2 and *EVS* values are close to 1, suggesting good prediction performance. In comparison with the random forest model developed by Almustafa & Nehdi [17] and Zhao et al. [19] for estimating the maximum displacement of RC slabs under explosive loads, the MLP model developed in this section exhibits better prediction performance, as proven by higher R^2 and *EVS* values, as well as a lower *SI* value. Larger *RMSE* and *MAE* in the MLP model are attributed to the higher average maximum displacement in the dataset. The average maximum displacement of the dataset in this study is 243.68 mm, which is significantly larger than those in the datasets used by Almustafa & Nehdi [17] and Zhao et al. [19], which are 33.38 mm and 34.55 mm, respectively.

Fig. 9 compares the predicted and actual displacements of the validation and test sets. In the ideal scenario, data points align along the red diagonal line, indicating a perfect agreement between the predicted and actual values. The green and purple dashed lines represent the error

Table 8
Performance of evaluation metrics on different datasets.

Data set	R^2	*EVS*	*RMSE*	*MAE*	*SI*
Training set	0.9929	0.9935	22.14	16.84	0.08586
Validation set	0.9886	0.9889	24.69	18.79	0.1157
Test set	0.9923	0.9922	18.46	16.11	0.0868

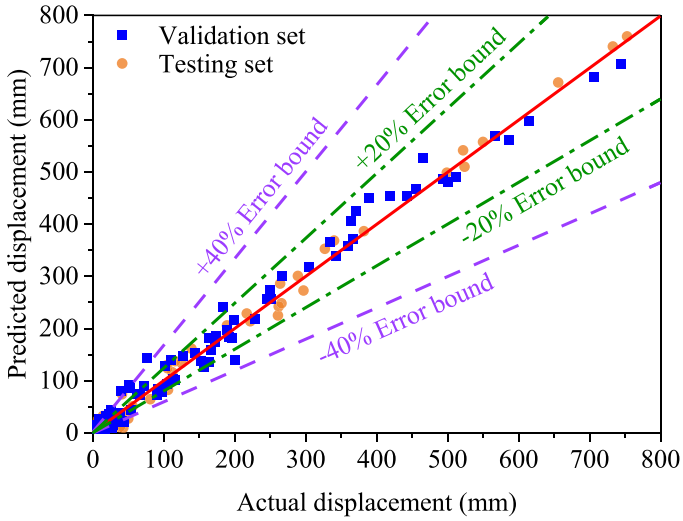

Fig. 9. Comparison between actual and predicted displacements.

margin of ± 20% and ± 40%, respectively. Most data points in the graph are located near the red line, showing that the predicted results are near the actual results. Further analysis is performed when the maximum displacement exceeds 50 mm considering the importance of larger displacements in assessing the maximum displacement of RC slabs under explosive loads. In the validation set, 57 samples with a maximum displacement exceed 50 mm. Among these, 48 data points fall within the ± 20% error margin, whereas 55 data points within the ± 40% error margin, accounting for 84.2% and 96.5% of the total, respectively. Similarly, in the test set, 31 samples have maximum displacements greater than 50 mm, with 27 data points falling within the ± 20% error margin and 30 data points falling within the ± 40% error margin, accounting for 87.1% and 96.8% of the total, respectively. The analysis indicates the developed MLP model is effective in assessing the maximum displacement of RC slabs under explosive loads in most cases.

3.3. Importance analysis of input features

The complexity of neural networks makes them black boxes. The intricate nonlinear relationship between input and output variables is challenging to explicitly express through empirical formulas. To gain deeper insights into the feature learning process of the model and to reveal the effects of each variable on the predicted result, permutation feature importance (PFI) analysis is used as an important interpretative technique [44]. When a relationship exists between input features and the target variable, shuffling the order of data within the input features affects the prediction errors, with a more pronounced effect as the correlation strengthens. A larger PFI value indicates that the feature plays a crucial role in predictions, while a smaller value implies less influence on the predictive outcomes.

Random permutations are applied to the 10 input features, and the PFI values are calculated based on RMSE for each input feature, as shown in Fig. 10. The highest PFI values are observed for charge mass M, blast distance d, slab types F, and slab thickness T, indicating that these four input features have the greatest influence on the output variable. In contrast, the concrete compressive strength f_c, spacing of reinforcement R, and rebar yield strength f_y have relatively minor effects on the predictive outcome of the model. The calculated relative importance of input features in this study is similar to the findings of Zhao et al. [19]. In their study, the most influential factors on prediction outcomes were charge mass, blast distance, and slab thickness, whereas the minor ones were the concrete compressive strength and rebar yield strength.

To verify the accuracy of the computed PFI results, a comprehensive

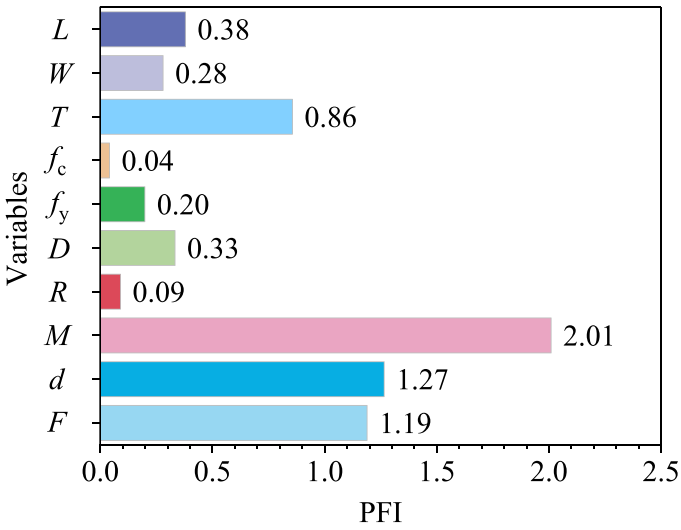

Fig. 10. Relative importance of input features.

parameter analysis is conducted utilizing collected literature data for charge mass M, blast distance d, slab thickness T, and concrete compressive strength f_c. Tables 9 to 12 present the influence of these four input features on the maximum displacement of RC slabs exposed to explosive loads. Table 9 shows that the charge mass remarkably affects the maximum displacement, with larger changes resulting in greater displacement changes. The influence of the blast distance on the maximum displacement is listed in Table 10. Notably, a reduction of 83% in the blast distance leads to a 1843% increase in maximum displacement. As indicated in Table 11, a reduction in the slab thickness is associated with diminished deformation resistance of the slab, resulting in an increase in its maximum displacement. In comparison with the three previously mentioned parameters, Table 12 shows that the influence of the concrete compressive strength on the maximum displacement is relatively small. The analysis suggests that the influence of the four aforementioned input features on the maximum displacement of RC slabs follows a sequence, that is, from stronger to weaker influence, consistent with the calculated PFI results. This affirms the reliability of the DL technique employed to estimate the maximum displacement of RC slabs under explosive loads.

4. Failure mode prediction models

A 1D-CNN model and five conventional ML models are developed to estimate the failure modes of RC slabs subjected to explosive loading. The training dataset consisted of 511 samples, with 270 single-way and 225 two-way slab samples. The number of samples exhibiting BF, SF, and BSF is 190, 135, and 186, respectively. The collected numerical simulation data samples lack information on their failure modes, hence, they are excluded from this section.

4.1. Configuration of models

(1) 1D-CNN model.

Table 9
Influence of charge mass.

Source	Charge mass (kg)	Change	Maximum displacement (mm)	Change
Wang et al. [28]	0.2	Base	10	Base
	0.31	55%	15	50%
	0.46	130%	35	250%
	0.55	175%	43	330%

Table 10
Influence of blast distance.

Source	Blast distance (m)	Change	Maximum displacement (mm)	Change
Syed et al. [7]	6	Base	0.7	Base
	3.15	48%	2	186%
	1	83%	13.6	1843%

Table 11
Influence of slab thickness.

Source	Slab thickness (mm)	Change	Maximum displacement (mm)	Change
Du & Li [31]	120	Base	6	Base
	110	8%	10	67%
	100	17%	12	100%
	90	25%	17	183%

Table 12
Influence of concrete compressive strength.

Source	compressive strength (MPa)	Change	Maximum displacement (mm)	Change
Du & Li [31]	54	Base	8.5	Base
	44	19%	9.5	12%
	34	37%	10.5	24%
	24	56%	12	41%

The classic CNN architecture was proposed by LeCun et al. [45] in 1989 and has been widely applied in various fields. As a multi-level feedforward DL algorithm, a typical CNN consists of two modules: the feature extraction part and the classification part. The feature extraction part typically consists of convolution-pooling-activation modules, filtering task-specific features from the input data, while the classification part is composed of fully connected layers, acting on the extracted features and assigning the probability for the input being a specific category. The 1D-CNN model is utilized in this section.

The setting of hyperparameters greatly influences the prediction performance of the 1D-CNN model. Thus, each hyperparameter value needs to be selected appropriately. In this section, the optimal hyperparameters are obtained by employing Bayesian optimization and 10-fold cross validation. After multiple comparisons and analyses, the hyperparameters for the 1D-CNN are determined as follows: the number of filters is set to 60, the kernel size is 2, the dense units are 224, the dropout rate is 0.15, and the activation function is ReLU. The 1D-CNN architecture is shown in Fig. 11. During the training process, the dropout regularization method [46] is employed to prevent the model from overly relying on specific local features, thereby enhancing its generalization ability.

(2) Traditional ML models.

Five traditional ML classification algorithms, namely, the k-nearest neighbors (KNN) algorithm, the light gradient boosting machine (LGBM) algorithm, the RF algorithm, the support vector classification (SVC) algorithm, and the extreme gradient boosting (XGBoost) algorithm, are utilized for comparison. They are trained on the same dataset as the comparative study with the 1D-CNN classification algorithm. Bayesian optimization is employed to obtain the optimal hyperparameters for each algorithm, followed by a 10-fold cross-validation to confirm their performance. The key hyperparameter settings for each algorithm are presented as follows:

- For the KNN algorithm, the number of neighbors is set to 1.

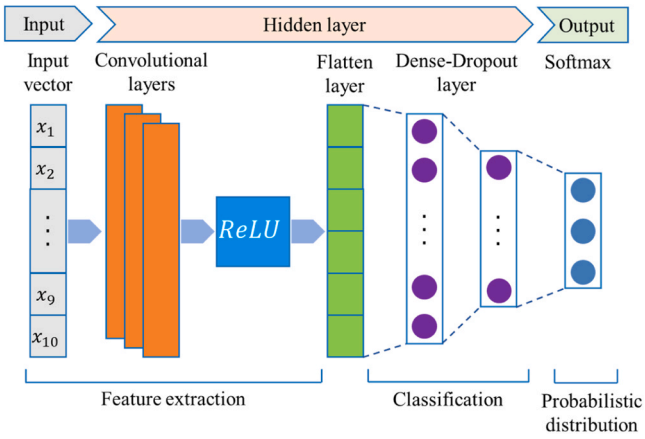

Fig. 11. Network structure of the 1D-CNN.

- For the LGBM algorithm, the number of leaves is 250, the learning rate is 0.0590, the minimum number of data points in a leaf is 34, and the minimum sum of Hessian in a leaf is 0.006925.
- For the RF algorithm, the number of estimators is 45, the maximum depth of each tree is 26, the minimum number of samples required to split an internal node is 3, and the minimum number of samples required to be at a leaf node is 3.
- For the SVC algorithm, the regularization parameter is 732.03, and the kernel coefficient for the radial basis function is 0.0792.
- For the XGBoost algorithm, the number of boosting rounds is 95, the maximum depth of a tree is 4, the learning rate is 0.2913, the minimum loss reduction required to make a further partition is 0.8324, and the fraction of features to be randomly sampled for each tree is 0.5103.

4.2. Analysis of training results

The prediction performance of the 1D-CNN model and five ML models is assessed using the 10-fold cross-validation technique. The dataset is split into 10 subsets, each of which is sequentially used as the validation set, whereas the rest are used for training the model [17]. This approach yields 10 distinct evaluations of model performance. The average of these 10 evaluation results serves as the performance metric, enabling a more reliable assessment of the model's generalization ability and prediction performance. This method helps avoid any potential instability that may arise from inappropriate data partitioning in the evaluation results.

Four assessment metrics, Accuracy, Precision, Recall, and F1-score, are used to assess the prediction performance of the model comprehensively. Accuracy represents the proportion of correctly predicted samples, while Precision assesses the proportion of true positive samples among all samples predicted as positive. Recall measures the ability of the model to predict all positive samples, and the F1-score combines Precision and Recall through their harmonic mean to evaluate their performance comprehensively. The formulas for these evaluation metrics are presented in Eqs. (6) to (9).

$$\text{Accuracy} = \frac{\text{TP} + \text{TN}}{\text{TP} + \text{FP} + \text{FN} + \text{TN}}, \tag{6}$$

$$\text{Precision} = \frac{\text{TP}}{\text{TP} + \text{FP}}, \tag{7}$$

$$\text{Recall} = \frac{\text{TP}}{\text{TP} + \text{FN}}, \tag{8}$$

$$\text{F1} - \text{score} = \frac{2 \times \text{Precision} \times \text{Recall}}{\text{Precision} + \text{Recall}}, \tag{9}$$

where TP and TN represent the number of samples correctly predicted as positive and negative classes, respectively; FP represents the number of samples incorrectly predicted as positive from the negative class, while FN represents the opposite scenario.

Table 13 presents the prediction performance of different algorithms on four metrics for various failure modes of RC slabs. The 1D-CNN model demonstrates commendable performance in predicting failure modes, with a prediction accuracy of 90%. Specifically, the BF and SF modes display superior performance, each achieving an F1-score of 92%. The prediction accuracy for the BSF mode is slightly lower, with an F1-score of 86%. This discrepancy can be attributed to the complexity of the BSF mode, which poses challenges to accurate prediction. Among the five ML algorithms, the SVC algorithm exhibits the highest prediction accuracy, achieving an accuracy rate of 86%. Following closely are the LGBM and XGBoost algorithms, with accuracy rates of 84%. In contrast, the prediction accuracy of the KNN algorithm is less satisfactory at only 75%. Upon examining the prediction outcomes of each algorithm for different failure modes, BF and SF exhibit better prediction performance than BSF. This outcome demonstrates the intricate nature of BSF, posing challenges for accurate prediction. Comparing traditional ML classification algorithms with the 1D-CNN model, the latter exhibits superior prediction performance across different failure modes.

Fig. 12 illustrates the application of the probability confusion matrix [47] in assessing the prediction performance of different failure modes of RC slabs. The values along the diagonal direction of the matrix indicate the probability of correct predictions for each specific category. With reference to the probability confusion matrix plot, a clear understanding of the specific prediction outcomes for each type of failure mode can be obtained. For the 1D-CNN model, the prediction results are presented as follows: In the case of the BF mode, 178 samples (94%) of the predictions are accurate, with 12 samples (6%) misclassified as BSF and none as SF. For the BSF mode, 160 (86%) are correct predictions, with 18 samples (10%) incorrectly classified as BF and 8 samples (4%) incorrectly classified as SF. Regarding SF, 121 correct predictions (90%) are made, with 14 samples (10%) misclassified as BSF and none as BF.

The prediction performance of each model is different. For the SVC algorithm, the accuracy rates for predicting BF and SF modes are 90% and 89%, respectively, with probabilities of misclassification into the BSF mode at 10% and 11%, respectively. In the BSF mode, the correct prediction probability is 81%, with probabilities of 11% and 8% for misclassifying as BF and SF modes, respectively. The overall prediction performance of the SVC algorithm is satisfactory. In contrast, the prediction performance of the KNN algorithm, particularly in predicting BSF and SF modes, is inadequate, with accuracy rates of only 66% and 67%, respectively. The LGBM, RF, and XGBoost algorithms exhibit

Table 13
Performance metrics of the 1D-CNN model and five ML models.

Algorithm	Failure mode	Precision	Recall	F1-score	Accuracy
1D-CNN	BF	0.91	0.94	0.92	0.90
	BSF	0.86	0.86	0.86	
	SF	0.94	0.90	0.92	
KNN	BF	0.73	0.91	0.81	0.75
	BSF	0.68	0.66	0.67	
	SF	0.93	0.67	0.78	
LGBM	BF	0.85	0.91	0.88	0.84
	BSF	0.80	0.74	0.77	
	SF	0.86	0.86	0.86	
RF	BF	0.85	0.87	0.86	0.81
	BSF	0.74	0.76	0.75	
	SF	0.86	0.79	0.83	
SVC	BF	0.90	0.90	0.90	0.86
	BSF	0.82	0.81	0.81	
	SF	0.88	0.89	0.89	
XGBoost	BF	0.86	0.89	0.88	0.84
	BSF	0.79	0.78	0.79	
	SF	0.88	0.84	0.86	

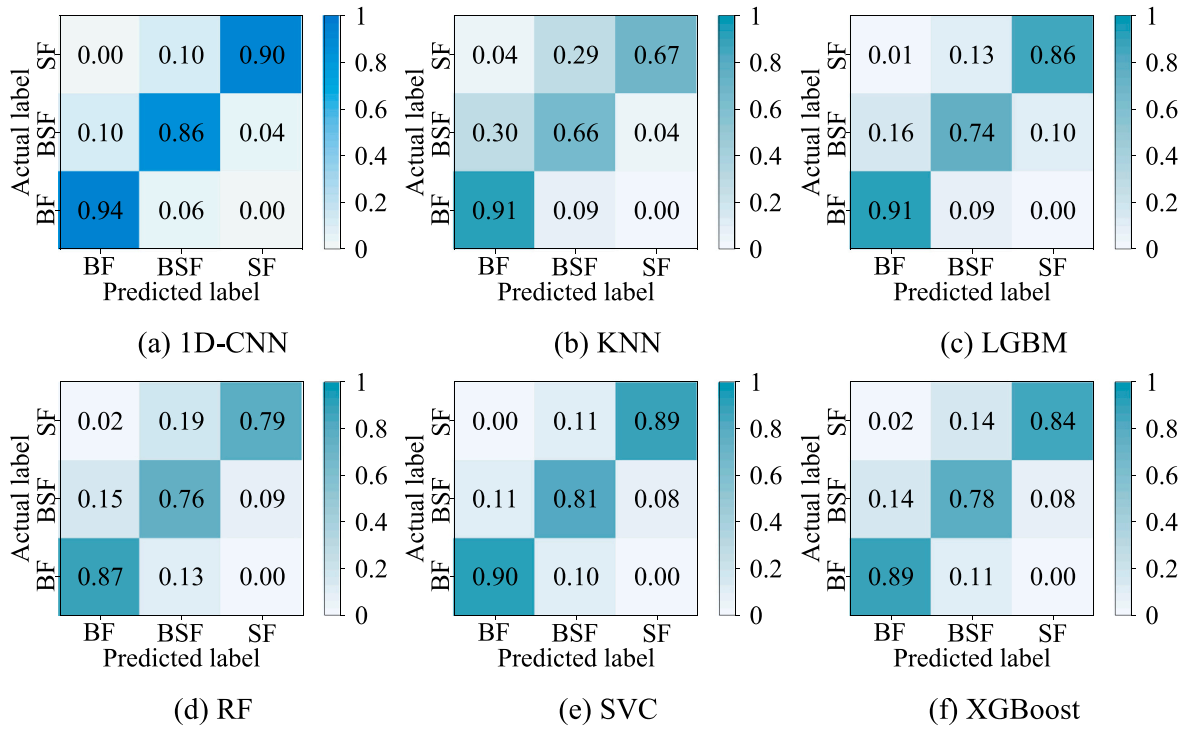

Fig. 12. Probabilistic confusion matrices of different algorithms.

comparable prediction performance across different failure modes, and their prediction abilities are acceptable. A comparative analysis demonstrates that the developed 1D-CNN algorithm outperforms traditional ML algorithms in terms of prediction performance. Therefore, the 1D-CNN model is selected as the prediction model for the failure mode of RC slabs under explosions.

4.3. PFI analysis of different algorithms

A PFI analysis was used to examine the influence of each input variable on the failure mode. This method evaluates the influence of individual input features on failure modes by rearranging the values of each feature and quantifying the effects of this permutation on the prediction performance. Fig. 13 shows the relative importance of each input feature for different algorithms. The four most important features in the 1D-CNN algorithm include charge mass M, blast distance d, slab type F, and slab thickness T. In contrast, the least significant feature is concrete compressive strength f_c.

The relative importance of features varies between algorithms among traditional ML algorithms. The SVC algorithm, which achieves the highest prediction accuracy, exhibits a similar feature relative importance ranking to the 1D-CNN algorithm, suggesting that both algorithms can efficiently extract features from the input data for this task, leading to superior prediction performance. In contrast, the KNN algorithm, which performs the worst in terms of prediction accuracy, struggles to extract meaningful features from the input data, leading to challenges in accurately predicting the failure modes of RC slabs under explosions. With regard to the LGBM, RF, and XGBoost algorithms, they demonstrate comparable prediction performance, as suggested by their similar feature importance rankings. Overall, the prediction performance of the model is closely related to its ability to extract features from the data, and strong feature extraction capabilities improve prediction performance. The analysis above shows that when dealing with the dataset of failure modes for RC slabs under explosive loads, the 1D-CNN algorithm possesses superior feature extraction capabilities compared with other algorithms.

5. Conclusions

In this study, two DL-based models for predicting the structural responses of RC slabs subjected to blast loads are developed. These models are trained and evaluated using collected literature data and supplemented numerical simulation data. The following conclusions can be drawn:

(1) The established MLP model demonstrates satisfactory predictive performance in assessing the maximum displacement of RC slabs under explosive loads. The prediction performance surpasses that of conventional ML models, with R^2 values for the training, validation, and test sets being 0.9929, 0.9886, and 0.9923, respectively. Relative importance analysis reveals that the charge mass and blast distance have the most remarkable effect on the maximum displacement of RC slabs, whereas the effect of concrete compressive strength is comparatively minor.

(2) The developed 1D-CNN model demonstrates higher prediction accuracy in forecasting the failure modes of RC slabs under explosions compared to five conventional ML classification models, achieving an improvement of 6–15%. The overall prediction accuracy of the 1D-CNN model is 90%, with accuracies of 94%, 90%, and 86% in predicting BF, SF, and BSF modes, respectively. The results demonstrate that the 1D-CNN model efficiently predicts the failure modes of RC slabs under explosive loads. Furthermore, the comparative PFI analysis indicates that the 1D-CNN model has superior feature extraction capabilities. Among the structural parameters, the type and thickness of the slab have a remarkable influence on the failure modes, whereas the compressive strength has a minor influence.

CRediT authorship contribution statement

Xiao-Qing Zhou: Conceptualization, Resources, Software, Writing – review & editing, Supervision. **Bing-Gui Huang:** Methodology, Formal analysis, Writing – original draft. **Xiao-You Wang:** Formal analysis, Writing – review & editing. **Yong Xia:** Writing – review & editing,

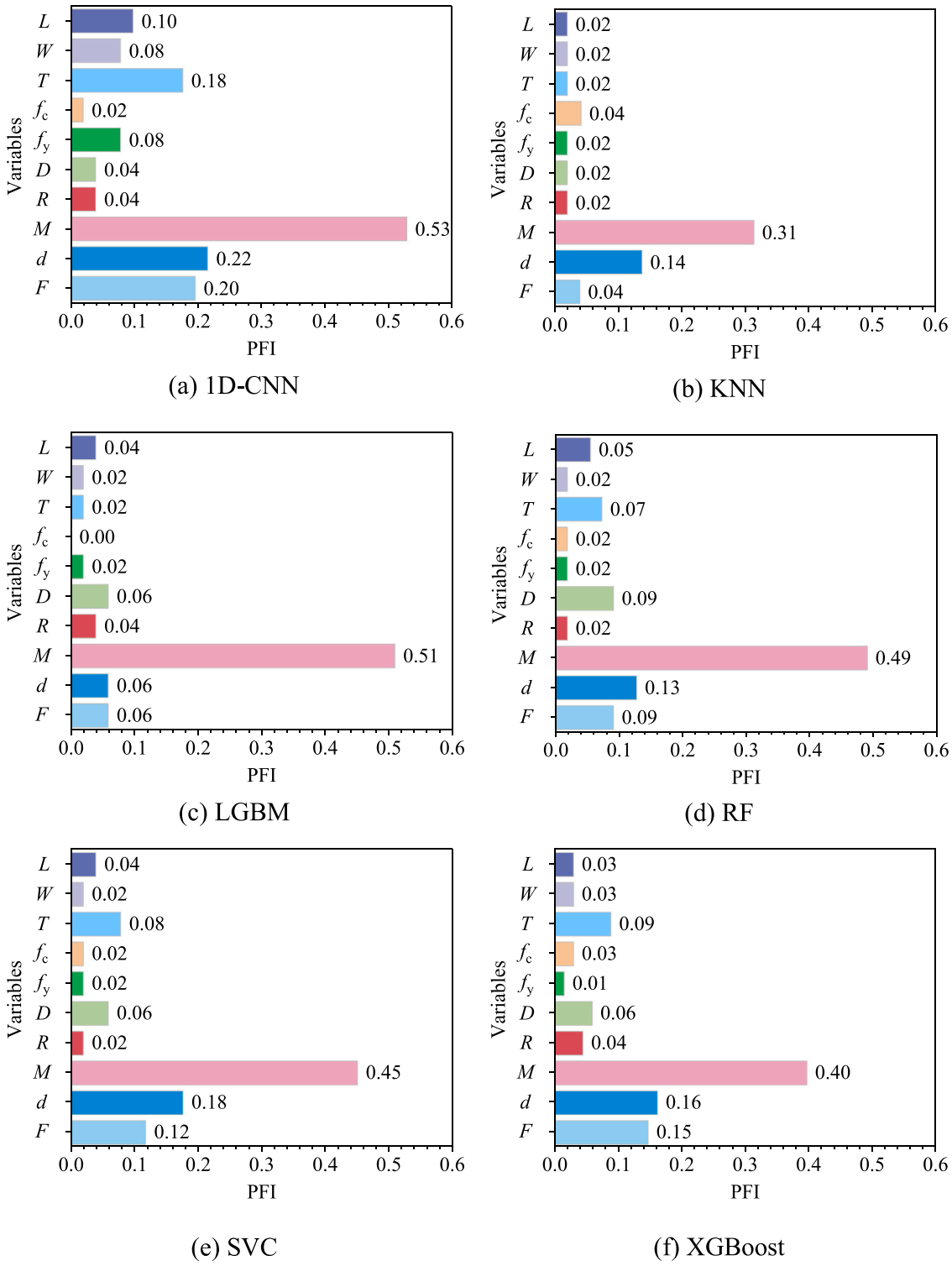

Fig. 13. Feature importance of different algorithms.

Funding acquisition, Supervision.

Declaration of Competing Interest

The authors declare that they have no known competing financial interests or personal relationships that could have appeared to influence the work reported in this paper.

Data Availability

Data will be made available on request.

Acknowledgments

The research was supported by the National Key Research and Development Program of China (Grant No. 2018YFB2100901).

References

[1] Anas SM, Alam M, Umair M. Experimental and numerical investigations on performance of reinforced concrete slabs under explosive-induced air-blast loading: a state-of-the-art review. Structures 2021;31:428–61. https://doi.org/10.1016/j.istruc.2021.01.102.

[2] Wang RY, Fang ZC, Lezgy-Nazargah M, Khosravi H. Nonlinear analysis of reinforced concrete slabs using a quasi-3D mixed finite element formulation. Eng Struct 2023;294:116781. https://doi.org/10.1016/j.engstruct.2023.116781.

[3] Li QM, Meng H. Pressure-impulse diagram for blast loads based on dimensional analysis and single-degree-of-freedom model. J Eng Mech 2002;128(1):87–92. https://doi.org/10.1061/(asce)0733-9399(2002)128:1(87).

[4] Wang W, Zhang D, Lu FY, Tang FJ, Wang SC. Pressure-impulse diagram with multiple failure modes of one-way reinforced concrete slab under blast loading using SDOF method. J Cent South Univ 2013;20(2):510–9. https://doi.org/10.1007/s11771-013-1513-z.

[5] Ma GW, Shi HJ, Shu DW. P–I diagram method for combined failure modes of rigid-plastic beams. Int J Impact Eng 2007;34(6):1081–94. https://doi.org/10.1016/j.ijimpeng.2006.05.001.

[6] El-Dakhakhni WW, Changiz Rezaei SH, Mekky WF, Razaqpur AG. Response sensitivity of blast-loaded reinforced concrete structures to the number of degrees of freedom. Can J Civ Eng 2009;36(8):1305–20. https://doi.org/10.1139/L08-140.

[7] Syed ZI, Raman SN, Ngo T, Mendis P, Pham T. The failure behavior of reinforced concrete panels under far-field and near-field blast effects. Structures 2018;14:220–9. https://doi.org/10.1016/j.istruc.2018.03.009.

[8] Zhou XQ, Kuznetsov VA, Hao H, Waschl J. Numerical prediction of concrete slab response to blast loading. Int J Impact Eng 2008;35(10):1186–200. https://doi.org/10.1016/j.ijimpeng.2008.01.004.

[9] Senthil K, Singhal A, Shailja B. Damage mechanism and stress response of reinforced concrete slab under blast loading. Couple Syst Mech 2019;8(4):315–38. https://doi.org/10.12989/csm.2019.8.4.315.

[10] Jia H, Yu L, Wu GY. Damage assessment of two-way bending RC slabs subjected to blast loadings. Sci World J 2014:718702. https://doi.org/10.1155/2014/718702.

[11] Zhao CF, Wang Q, Lu X, Wang J. Numerical study on dynamic behaviors of NRC slabs in containment dome subjected to close-in blast loading. Thin Wall Struct 2019;135:269–84. https://doi.org/10.1016/j.tws.2018.11.013.

[12] Li ZX, Shi YC, Shi XS. Damage analysis and assessment of RC slabs under blast load. J Build Eng 2009;30(6):60–6.

[13] Lai DD, Demartino C, Xiao Y. Interpretable machine-learning models for maximum displacements of RC beams under impact loading predictions. Eng Struct 2023;281:115723. https://doi.org/10.1016/j.engstruct.2023.115723.

[14] Jueyendah S, Lezgy-Nazargah M, Eskandari-Naddaf H, Emamian SA. Predicting the mechanical properties of cement mortar using the support vector machine approach. Constr Build Mater 2021;291:123396. https://doi.org/10.1016/j.conbuildmat.2021.123396.

[15] Naderpour H, Mirrashid M, Parsa P. Failure mode prediction of reinforced concrete columns using machine learning methods. Eng Struct 2021;248:113263. https://doi.org/10.1016/j.engstruct.2021.113263.

[16] Li QL, Wang ZT, Li L, Hao H, Chen WS, Shao YD. Machine learning prediction of structural dynamic responses using graph neural networks. Comput Struct 2023;289:107188. https://doi.org/10.1016/j.compstruc.2023.107188.

[17] Almustafa MK, Nehdi ML. Machine learning model for predicting structural response of RC slabs exposed to blast loading. Eng Struct 2020;221:111109. https://doi.org/10.1016/j.engstruct.2020.111109.

[18] Almustafa MK, Nehdi ML. Machine learning prediction of structural response for FRP retrofitted RC slabs subjected to blast loading. Eng Struct 2021;244:112752. https://doi.org/10.1016/j.engstruct.2021.112752.

[19] Zhao CF, Zhu YF, Zhou ZH. Machine learning-based approaches for predicting the dynamic response of RC slabs under blast loads. Eng Struct 2022;273:115104. https://doi.org/10.1016/j.engstruct.2022.115104.

[20] Azimi M, Eslamlou AD, Pekcan G. Data-driven structural health monitoring and damage detection through deep learning: State-of-the-art review. Sensors 2020;20(10):2778. https://doi.org/10.3390/s20102778.

[21] Fan G, Li J, Hao H. Lost data recovery for structural health monitoring based on convolutional neural networks. Struct Control Hlth 2019;26(10):e2433. https://doi.org/10.1002/stc.2433.

[22] Khallaf R, Khallaf M. Classification and analysis of deep learning applications in construction: a systematic literature review. Autom Constr 2021;129:103760. https://doi.org/10.1016/j.autcon.2021.103760.

[23] Deng FM, He YG, Zhou SX, Yu Y, Cheng HG, Wu X. Compressive strength prediction of recycled concrete based on deep learning. Constr Build Mater 2018;175:562–9. https://doi.org/10.1016/j.conbuildmat.2018.04.169.

[24] Zhou SX, Sheng W, Wang ZP, Yao W, Huang HW, Wei YQ, et al. Quick image analysis of concrete pore structure based on deep learning. Constr Build Mater 2019;208:144–57. https://doi.org/10.1016/j.conbuildmat.2019.03.006.

[25] Wei YG, Yang QL, Wang TT, Jiang CS, Bian YJ. Earthquake and explosion identification based on Deep Learning residual network model. Acta Seismol Sin 2019;41(5):646–57. https://doi.org/10.11939/jass.20190030.

[26] Zhou XQ, Huang BG, Wang XY, Xia Y. Deep learning-based rapid damage assessment of RC columns under blast loading. Eng Struct 2022;271:114949. https://doi.org/10.1016/j.engstruct.2022.114949.

[27] Yao SJ, Zhang D, Chen XG, Lu FY, Wang W. Experimental and numerical study on the dynamic response of RC slabs under blast loading. Eng Fail Anal 2016;66:120–9. https://doi.org/10.1016/j.engfailanal.2016.04.027.

[28] Wang W, Zhang D, Lu FY, Wang SC, Tang FJ. Experimental study and numerical simulation of the damage mode of a square reinforced concrete slab under close-in explosion. Eng Fail Anal 2013;27:41–51. https://doi.org/10.1016/j.engfailanal.2012.07.010.

[29] Wang W, Zhang D, Lu F, Wang SC, Tang FJ. Experimental study on scaling the explosion resistance of a one-way square reinforced concrete slab under a close-in blast loading. Int J Impact Eng 2012;49:158–64. https://doi.org/10.1016/j.ijimpeng.2012.03.010.

[30] Wu C, Oehlers DJ, Rebentrost M, Leach J, Whittaker AS. Blast testing of ultra-high performance fibre and FRP-retrofitted concrete slabs. Eng Struct 2009;31(9):2060–9. https://doi.org/10.1016/j.engstruct.2009.03.020.

[31] Du H, Li ZX. Numerical analysis of dynamic behavior of RC slabs under blast loading. Trans Tianjin Univ 2009;15(1):61–4. https://doi.org/10.1007/s12209-009-0012-7.

[32] Abdel-Mooty M, Alhayawei S, Issa M. Numerical evaluation of the performance of two-way RC panels under blast loads. Struct Shock Impact SUSI XIII 2014:13–25. https://doi.org/10.2495/SUSI140021.

[33] Su Q, Wu H, Sun HS, Fang Q. Experimental and numerical studies on dynamic behavior of reinforced UHPC panel under medium-range explosions. Int J Impact Eng 2021;148:103761. https://doi.org/10.1016/j.ijimpeng.2020.103761.

[34] Malvar LJ, Crawford JE, Wesevich JW, Simons D. A plasticity concrete material model for DYNA3D. Int J Impact Eng 1997;19(9-10):847–73. https://doi.org/10.1016/S0734-743X(97)00023-7.

[35] Bischoff PH, Perry SH. Compressive behavior of concrete at high strain rates. Mater Struct 1991;24:425–50. https://doi.org/10.1007/BF02472016.

[36] Malvar L.J., Crawford J.E. Dynamic increase factors for concrete. In: 28th Department of Defense Explosives Safety seminar, Orlando, FL; 1998, p. 1–17.

[37] Hallquist J.L.S.-DYNA theory manual – ls971. Technical report. Livermore, California, USA: Livemore Software; 2007.

[38] Malvar L.J., Crawford J.E. Dynamic Increase Factors for Steel Reinforcing Bars. In: 28th DDESB Seminar, Orlando, USA; 1998, p. 1–18.

[39] FEMA 426 Reference manual to mitigate potential terrorist attacks against buildings. Federal Emergency Management Agency; 2003 . .

[40] Chinese Standard. GB 50010–2010. Code for design of concrete structures. Beijing: China Planning Press; 2010. (in China).

[41] Wu J, Chen XY, Zhang H, Xiong LD, Lei H, Deng SH. Hyperparameter optimization for machine learning models based on Bayesian optimization. J. Electron. Sci Technol 2019;17(1):26–40. https://doi.org/10.11989/JEST.1674-862X.80904120.

[42] Wong TT, Yeh PY. Reliable accuracy estimates from k-fold cross validation. IEEE Trans Knowl Data Eng 2019;32(8):1586–94. https://doi.org/10.1109/TKDE.2019.2912815.

[43] Timur Cihan M. Prediction of concrete compressive strength and slump by machine learning methods. Adv Civ Eng 2019;2019:1–11. https://doi.org/10.1155/2019/3069046.

[44] Strobl C, Boulesteix AL, Kneib T, Augustin T, Zeileis A. Conditional variable importance for random forests. BMC Bioinform 2008;9:1–11. https://doi.org/10.1186/1471-2105-9-307.

[45] LeCun Y, Boser B, Denker JS, Henderson D, Howard RE, Hubbard W, et al. Backpropagation applied to handwritten zip code recognition. Neural Comput 1989;1(4):541–51. https://doi.org/101162/neco.1989.1.4.541.

[46] Srivastava N, Hinton G, Krizhevsky A, Sutskever I, Salakhutdinov R. Dropout: a simple way to prevent neural networks from overfitting. J Mach Learn Res 2014;15(1):1929–58.

[47] Nguyen KTP, Medjaher K. A new dynamic predictive maintenance framework using deep learning for failure prognostics. Reliab Eng Syst Safe 2019;188:251–62. https://doi.org/10.1016/j.ress.2019.03.018.